

Mobility of non-exhaust brake wear dust from road traffic in saturated and unsaturated porous media mimicking subsurface environments

Original

Mobility of non-exhaust brake wear dust from road traffic in saturated and unsaturated porous media mimicking subsurface environments / Acocella, M., Bianco, C., Tosco, T., Sethi, R.. - In: JOURNAL OF HAZARDOUS MATERIALS. - ISSN 0304-3894. - 491:(2025). [10.1016/j.jhazmat.2025.137851]

Availability:

This version is available at: 11583/2998329 since: 2025-03-17T15:28:05Z

Publisher:

Elsevier

Published

DOI:10.1016/j.jhazmat.2025.137851

Terms of use:

This article is made available under terms and conditions as specified in the corresponding bibliographic description in the repository

Publisher copyright

(Article begins on next page)



Mobility of non-exhaust brake wear dust from road traffic in saturated and unsaturated porous media mimicking subsurface environments

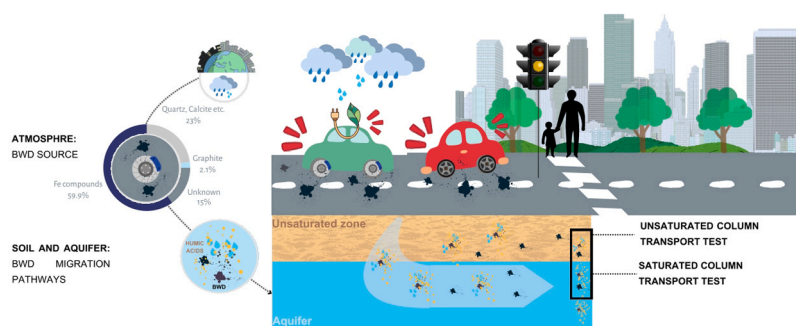
Michela Acocella , Carlo Bianco , Tiziana Tosco *, Rajandrea Sethi

Department of Environment, Land and Infrastructure Engineering (DIATI) & Clean Water Center (CWC), Politecnico di Torino, Corso Duca degli Abruzzi, 24, Turin 10129, Italy

HIGHLIGHTS

- Brake wear dust (BWD) is a key non-exhaust emission (NEE) in urban pollution.
- BWD moves through both unsaturated and saturated porous media.
- Soil type and water flow dynamics influence BWD environmental behavior.
- Metals in BWD threaten soil and groundwater quality in urban environments.

GRAPHICAL ABSTRACT



ARTICLE INFO

Keywords:

Traffic non-exhaust emissions
Brake wear dust
Particle transport in porous media
Urban pollution
Soil contamination
Groundwater contamination

ABSTRACT

Road traffic is a major source of atmospheric pollution, especially in urban areas, contributing significantly to particulate matter (PM) emissions. While electric vehicles (EVs) help reduce exhaust emissions, they do not substantially address non-exhaust emissions (NEEs), such as brake wear dust (BWD), which remains a significant source of PM, particularly in urban environments. This study investigates at a preliminary level the environmental fate of BWD, studying at the laboratory scale its mobility and behaviour in unsaturated and saturated porous media, which simulate subsoil and aquifer conditions. BWD, produced through friction between brake pads and rotors during deceleration, can settle on road surfaces, posing risks to soil and water quality through runoff and infiltration. Laboratory tests were conducted here to highlight BWD transport mechanisms in porous media. BWD mobility is influenced by ionic strength and flow velocity, with higher rates promoting particle transport, and higher ionic strengths inhibiting it. The study also highlights the importance of soil composition, with sandy soils allowing for greater BWD mobility than clay-rich soils. The findings evidence the need for continued research to better understand the environmental risks posed by BWD, particularly in unsaturated soils. Additionally, the potential of BWD to act as a carrier for other pollutants requires further investigation.

* Corresponding author.

E-mail address: tiziana.tosco@polito.it (T. Tosco).

<https://doi.org/10.1016/j.jhazmat.2025.137851>

Received 6 December 2024; Received in revised form 20 February 2025; Accepted 3 March 2025

Available online 4 March 2025

0304-3894/© 2025 The Author(s). Published by Elsevier B.V. This is an open access article under the CC BY-NC-ND license (<http://creativecommons.org/licenses/by-nc-nd/4.0/>).

1. Introduction

Road traffic is a major contributor to atmospheric pollution, especially in urban areas, and hence to particulate matter (PM) emissions, which pose substantial risks to human health and are linked to premature deaths worldwide [1,2]. Current strategies and policies toward a more sustainable road mobility in Europe are fuelling the adoption of hybrid and electric vehicles (EVs) instead of conventional internal combustion engine vehicles (ICEVs) [3,4]. The transition to EVs is reducing exhaust emissions (EEs) (such as nitrogen oxides, exhaust PM, carbon monoxide, unburned hydrocarbons and volatile organic compounds), but the growing number of circulating vehicles, proportional to population urbanization and growth, and the generally heavier weight of EVs compared to ICEVs, is not leading to a significant reduction of non-exhaust emissions (NEEs) from sources such as brake, tire and road pavement wear [5-7]. Literature studies evidenced a potential increase of PM10 and PM2.5 emissions from EVs compared to ICEVs and change in composition [8]. In particular heavier EVs are expected to increase non-exhaust PM2.5 by 3–8 % relative to conventional vehicles [9,10].

Among NEEs, brake wear dust (BWD) is the most abundant non-exhaust particulate measured in urban areas [11,12], accounting for 16 % - 55 % of PM10 from road traffic [13-15]. Piscitello et al. [1] highlight that brake wear PM10 emission factors range from $1 \text{ mg km}^{-1} \text{ veh}^{-1}$ to $18.5 \text{ mg km}^{-1} \text{ veh}^{-1}$. In modern passenger cars, disc brake systems are commonly used, employing flat brake pads that exert pressure against a rotating metal disc. Grey cast iron is typically the material of rotors, while the brake linings consist of five primary components: binders, fibres, fillers, frictional additives or lubricants, and abrasives [13]. The frictional heat generated during braking events leads to the wear of linings and rotors, producing micronized particles [1,16]. Moreover, a nanocrystalline layer of iron oxides, produced by oxidative mild wear of the cast iron disc and by oxidation of low metallic pads, is formed at the contact surface between brake pad and rotor, and contributes to debris formation [17]. The resulting particles vary in size, mass and chemical composition, making their characterization challenging [18].

The current substantial lack of standardized sampling and measuring procedures leads researchers to use different experimental and analytical approaches, which produce hardly comparable results [13]. According to Kumar & Ghosh [19], the dimension of brake wear particles ranges from a few nanometres up to $100 \mu\text{m}$. Despite variations in brake material among manufacturers, Fe, Cu, Zn, Ba and Sb are consistently attributed to brake wear and thus used as markers for brake debris [20, 21,14,22,23]. Liati et al. [23], using energy dispersive X-ray analyses of particles collected on a brake test bench, found that Fe is dominant in every size fraction, confirming the magnetic nature of debris [16]. However, the NEEs characterization studies are strongly affected by variables such as test conditions, traffic intensity, road characteristics, and climate factors [1].

The current lack of generalizable values of size, composition and consequently of characterization procedures and protocols is probably the first cause of the absence of universal emission limits of wear particles from vehicles and roads in Europe [24].

It is evident, at this point, that BWD represents an emerging contaminant and a source of potential risk to human health and different environmental domains. The contamination of soils by heavy metals in proximity to roads has been already evidenced in the literature [25-27]. Depending on their size, brake wear particles can be either airborne or sedimentary. Airborne particles, dispersed and suspended in the air, can undergo atmospheric deposition (wet and/or dry) and reach the ground. Non-airborne particles may deposit on road surface or be attracted onto car wheels [28]. Both may be washed away by rain, contaminating urban or highway stormwater runoff, and thus the receiving surface water [7,29]. Ultimately, following infiltration, they can contribute to subsoil and groundwater contamination. Despite these risks, knowledge gaps remain concerning their migration pathways subsequent to

atmospheric deposition and/or rainwater interception, as well as their interaction with substances such as humic acids, potentially able to reduce aggregation and instability of such colloids, thus facilitating their leaching [30-32].

This study aims to contribute to fill this knowledge gap by investigating the key properties and mechanisms controlling the transport of brake wear particles in unsaturated and saturated porous media, representative of the unsaturated zone and the aquifer, respectively. Despite the well-consolidated knowledge on the mechanisms and key factors controlling colloid transport in porous media, specific studies are needed, like the one we present here, to elucidate the specific behavior of BWD: being highly heterogenous in size, morphology and composition, its transport in the subsoil cannot be approximated a-priori by referring to general colloid transport theories. The chemical composition and morphology of real BWD samples were analysed using different techniques (SEM-EDX, Raman spectroscopy, ICP-MS). Column transport tests were conducted under saturated and unsaturated conditions, investigating the impact of flow velocity and ionic strength on particle mobility and accumulation in the columns mimicking subsurface environment. These experimental results were then modeled using colloid transport software to provide preliminary insights into the key mechanisms and critical factors influencing BWD migration through the sub-surface, which can guide further studies at the field scale.

2. Materials and methods

2.1. Brake wear dust: characterization and suspension preparation

A sample of brake wear residues accumulating on wheel rims and braking systems was collected from cars of various brands and cylinder capacities in a workshop with service of changing tyres. The BWD sample was subjected to subsequential sieving to retain only fine particles with dimensions lower than $45 \mu\text{m}$, since larger particles are not expected to exhibit any mobility in soil and aquifer systems.

To determine particles size, morphology, and elemental composition of the BWD sample, SEM-EDS microscopy (FEI instrument – Hillsbor, OR) was used. A suspension of BWD in deionized water (50 mg/l) was filtered on a polycarbonate membrane ($0.4 \mu\text{m}$ pore size), air-dried and deposited on the stubs. The obtained SEM images were processed using the software ImageJ [33] to evaluate the particle size distributions. A further characterization in terms of chemical composition was obtained by means of a confocal Raman microscope (inVia™ – Renishaw – UK) equipped with 532 nm laser excitation. Moreover, the concentration of several metals was determined by an external laboratory (EUROLAB srl - Italy). The protocol included microwave assisted digestion of the sample (EPA method 3051 A) followed by inductivity coupled plasma–mass spectrometry (ICP–MS, EPA method 6020B).

A suspension was prepared by dispersing BWD in deionized water to a concentration of 2000 mg/L . To effectively disperse the particles, the sample was sonicated for at least 10 minutes in an ultrasonicator bath (CEIA CP102 - Italy). Then, it was stirred for 12 hours through a magnetic stirrer (Thermo Scientific Cimarec I – Walton-on-the-Naze – UK). After a second step of sonication (10 minutes), the particles were coated by humic acid (HA) (Humic acid sodium salt, tech. 50–60 % as humic acid – Alfa Aesar) at the initial concentration of 0.04 g/L , to mimic the HA coating that can naturally occur for BWD (as well as other particles) when dispersed in the subsoil. The suspension was then stirred for 12 hours and then centrifugated at 8000 rpm for 15 min (Neya 16 centrifuge – Remi Elektrotechnik Ltd – India) to eliminate the exceeding humic acid. We measured a residual concentration of humic acid equal to 0.0275 mg/L through a TOC analyzer (TOC-LDSH FA, E200, Shimadzu – Milan, Italy). The calibration curve TOC (total organic carbon) – HA used for this calculation is provided in Figure S 1 in [Supporting Information](#) (SI). The centrifuged part was then resuspended in either deionized water (DIW) (for column transport tests performed in both unsaturated and saturated conditions) or rainwater (RW) (for tests in

saturated conditions). Thanks to careful handling of the samples, a final BWD concentration of 2 g/L was achieved in both waters. The RW was collected in Turin rejecting the first rain (at least 10 minutes), and then filtered to remove any impurities. The RW underwent a chemical analysis performed by an external laboratory (EUROLAB srl – Italy) and its ionic strength (IS) resulted equal to 5 mM. The complete analysis of RW and the calculation of IS are provided in Table S 1 in SI.

BWD coated with HA was characterised by zeta potential values of -13.2 ± 0.4 mV in DIW and -17.2 ± 0.4 mV in RW, measured by dynamic light scattering (DLS Zetasizer Nano Z – Malvern Instruments Ltd – UK).

2.2. Column transport tests: experimental and analytical protocol

The transport experiments were performed in adjustable-height Plexiglas columns with 1.6 cm inner diameter and adjustable length. Three porous media were used, namely silica sand and two standard soils. Silica sand (Dorsilit 8, Dorfner, Germany; d_{10} , d_{50} and d_{90} equal respectively to 0.415, 0.45 and 0.5 mm) was used as a reference porous medium for both saturated and unsaturated tests. Before column packing, the sand was cleaned applying three sequential cycles of washing and sonication with 100 mM NaOH, tap water and deionized water, respectively, to remove any impurities and colloids [34]. After the cleaning procedure, the sand was dried in the oven and stored. For unsaturated column transport tests, two additional standard soils were also used, namely a sandy loam soil (LUFA 2.2) and clayey loam soil (LUFA 2.4, LUFA Speyer – Germany). The nominal soil grain size distribution is equal to 10.8 % for $d < 0.002$ mm, 15.7 % for $0.02 < d < 0.05$ mm, 73.5 % for $0.05 < d < 2$ mm (for LUFA 2.2), 23.7 % for $d < 0.002$ mm, 42.2 % for $0.02 < d < 0.05$ mm, 33.1 % for $0.05 < d < 2$ mm (for LUFA 2.4).

2.2.1. Column transport tests in saturated conditions

A scheme of the experimental setup is illustrated in Fig. 1 (a). For each column, 35 g of dry sand were re-hydrated and used to wet-pack the column to a height of 10 cm with vibration to minimize any layering or air entrapment, following the procedure detailed in [35]. First, a tracer test, aimed at determining porosity and dispersivity of each column, was performed injecting a 10 mM NaCl solution for at least 3 pore volumes (PVs) at constant rate, followed by flushing with deionized water (DIW) until the breakthrough curve (BTC) was completely exhausted, to ensure the absence of solute. Following the protocol of Bianco et al., [36], the tracer concentration at the column outlet was monitored in-line every 10 s using a UV-vis spectrophotometer (Specord S600, Analytik Jena, Germany) equipped with flow-through cells characterized by a 2 mm light path (Hellma, Germany) at a wavelength of

198.5 nm (which showed linear relationship between absorbance and concentration).

The BTC was fitted to the classical advection-dispersion equation (1) using the software MNMs 2021 (www.polito.it/ricerca/groundwater/it/software/mnms) [37]:

$$n \frac{\partial c_t}{\partial t} = \alpha_{sat} q \frac{\partial^2 c_t}{\partial x^2} - q \frac{\partial c_t}{\partial x} \quad (1)$$

where c_t is the tracer concentration [ML^{-3}], α_{sat} is the dispersivity [L], q is the Darcy velocity [LT^{-1}], and n is the effective porosity of the packed bed [-]. An average porosity n of 0.41 ± 0.04 and average dispersivity α_{sat} of $(1.33 \pm 0.3) \cdot 10^{-3}$ m for the sand (Table 3), and of 0.37 ± 0.03 and of $(5.00 \pm 2) \cdot 10^{-4}$ m for the soils were obtained, respectively (Table 5).

After the tracer test, the experimental procedure included the following steps: (i) column equilibration (5 PVs) with the same water used for the BWD suspension preparation (namely, DIW or RW); (ii) injection of BWD particles suspended either in DIW or in RW (10 PVs); (iii) first flushing (10 PVs) with the background water; (iv) second flushing (10 PVs) with DIW; (v) last flushing (10 PVs) with 3 mM NaOH solution to force the mobilization of possible reversibly attached particles.

All experiments were performed injecting the solutions and suspensions with a peristaltic pump, with top-to-bottom configuration, at three different injection rates (0.56, 1.07, 1.93 mL/min), corresponding respectively to Darcy velocities $q_1 = 4.01$, $q_2 = 7.66$ and $q_3 = 13.82$ m/d, which were maintained constant for the entire duration of the experiment.

During the tests, the column outflow was collected using a fraction collector (3 samples per PV). Based on particle characterization, iron was identified as the main metal tracer of BWD, thus the particle concentration was determined measuring the magnetic susceptibility of the collected samples, thanks to the linear relationship between concentration and susceptibility [38]. The calibration curve is reported in Supporting Information in Figure S2. More specifically, the BWD breakthrough curve was determined by measuring the magnetic susceptibility of the aqueous samples of the fraction collector using an MS2 magnetic susceptibility sensor (Bartington Instruments – UK). The concentration profiles (mass of particles per unit mass of porous medium as a function of the position along the column) were determined following two approaches. First, the profile was determined at the end of each injection step of the test using a core logging susceptibility sensor (Bartington Instruments – UK), positioned coaxially to the column and moved along it for recording the susceptibility with a space interval of 1 cm (Fig. 1(a)). An algorithm was used for the spatial decorrelation of

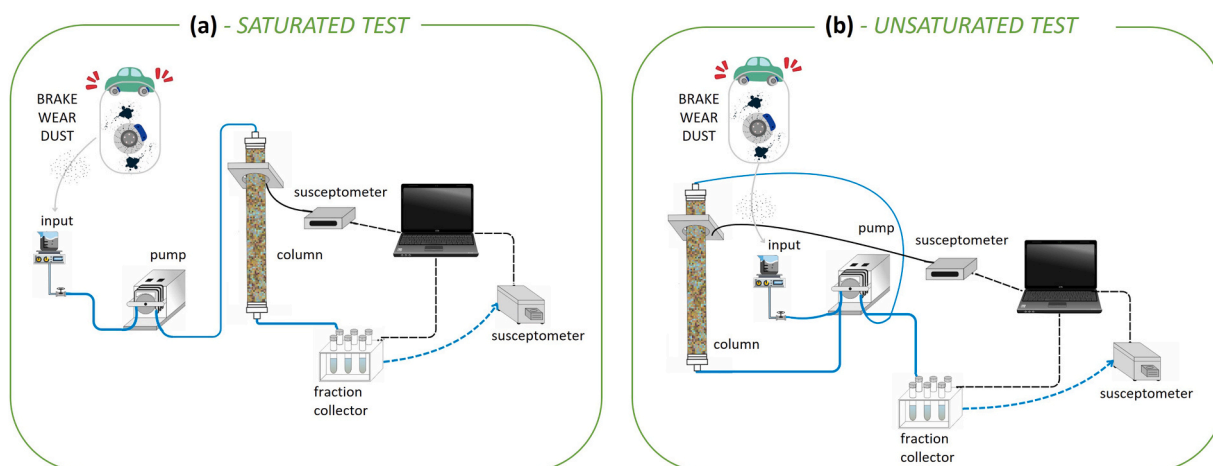


Fig. 1. Experimental setup for BWD transport tests – (a) saturated conditions; (b) unsaturated conditions.

the raw signal [38]. Additionally, at the end of the test the column was extruded and divided in 1 cm-long sand aliquots. The samples were then suspended in 5 mL of DIW and sonicated for 10 min to promote detachment of retained particles. The supernatant was then analysed with the sensor, and a scale factor was applied to convert the susceptibility measured by the core sensor into BWD mass in each sample and, being the sand mass known, into BWD concentration in solid phase. The scale factor was obtained by imposing equal total BWD mass retained in the column for the concentration profile measured by the susceptibility sensor at the end of the column test and obtained from column dissection.

2.2.2. Column transport tests in unsaturated conditions

The same procedure detailed for saturated columns was adopted for the preparation of the sand-packed columns used for the unsaturated transport tests and for the determination of porosity and saturated hydrodynamic dispersivity (Table 5). Conversely, for the transport tests performed in standard soils, the columns were packed dry: 30 g of dry soil were introduced and compacted with a pestle layer by layer until reaching a column height of 10 cm. After packing, an upward flux was established at a rate lower than 0.15 cm/min using a peristaltic pump (Ismatec ms-4/06 Reglo – USA) until soil saturation [39], followed by downward flushing with deionized water at the same rate until removing all the residual mobile soil colloids from the column. The flow was maintained until the outflow was visibly clear. The tracer test in saturated conditions was then performed.

After the saturated tracer test, the columns were drained by gravity until field capacity was reached. During drainage, the released water was collected and weighted, obtaining a measure of the gravitational water. Once desaturation was completed, steady state (unsaturated) flow was re-established by feeding the columns at fixed flow rate (either Q_1 or Q_3 for sand-packed columns, Q_3 for soil-packed columns, depending on the test). Both inlet (top) and outlet (bottom) of the column were attached to the peristaltic pump to ensure a water extraction with the same inlet flow rate. In this way, a constant water content vertical profile was guaranteed at steady state.

A second tracer test in unsaturated conditions was then run to determine water content and unsaturated dispersivity, estimated via least-squares fitting of the BTC to the classical advection-dispersion equation (2) in unsaturated porous media using Hydrus 1D [40]:

$$\theta \frac{\partial c_t}{\partial t} = \alpha_{unsat} q \frac{\partial^2 c_t}{\partial x^2} - q \frac{\partial c_t}{\partial x} \quad (2)$$

where α_{unsat} is the dispersivity in unsaturated conditions [L], and θ is the volumetric water content [-].

Average water content of 0.28 and average unsaturated dispersivity of $(5.10 \pm 1.4) \cdot 10^{-3}$ m for the sand, and of 0.31 ± 0.01 and of $(8.5 \pm 2.1) \cdot 10^{-3}$ m for the soils were obtained, respectively (Table 5).

The experimental procedure of BWD transport tests in unsaturated conditions followed the same protocol adopted for saturated columns, except for the flushing with NaOH, which was not performed. Also, the breakthrough curves and the profiles of retained particles were determined following the same approach previously described. A scheme of the experimental setup is illustrated in Fig. 1 (b).

2.2.3. Numerical modelling of BWD transport

The particle transport in porous media is usually modelled by a modified advection-dispersion equation, that for one-dimensional homogeneous systems can be written as [41,42]:

$$\begin{cases} \theta \frac{\partial c}{\partial t} + \rho_b \frac{\partial s}{\partial t} = \alpha q \frac{\partial^2 c}{\partial x^2} - q \frac{\partial c}{\partial x} \\ \rho_b \frac{\partial s}{\partial t} = f(c, t) \end{cases} \quad (3)$$

where c is the colloid concentration in the liquid phase [ML⁻³], s is the

colloid concentration retained on the solid phase [MM⁻¹], ρ_b is the bulk density of the solid matrix [ML⁻³], α is either the dispersivity in saturated conditions (α_{sat}) or unsaturated conditions for the given θ (α_{unsat}). The second equation describes the mass exchanges between the liquid and the solid phase with a generic formulation f . In this work, a qualitative analysis of the shape of BWD breakthrough curves suggested the mechanical filtration to be the dominant process along with reversible deposition controlled by physical-chemical interactions. Thus, two concurrent interaction sites were considered, corresponding to an irreversible (*site 1*) and reversible (*site 2*) linear deposition, respectively:

$$\begin{cases} \rho_b \frac{\partial s_1}{\partial t} = nk_{a,1}c \\ \rho_b \frac{\partial s_2}{\partial t} = nk_{a,2}c - \rho_b k_{d,2}s \end{cases} \quad (4)$$

where $k_{a,i}$ and $k_{d,i}$ are, respectively, the attachment and detachment coefficients for the i -th site [T⁻¹].

For tests in saturated conditions, the particle transport parameters were obtained by fitting the results of the part of the BTC corresponding to the injection and first flushing using MNMs 2021 (www.polito.it/ricerca/groundwater/it/software/mnms) [37] using space and time steps respectively equal to $\Delta x = 0.0005$ m and $\Delta t = 2$ s. The transport equation under unsaturated conditions was solved using Hydrus 1D [40] with space and time steps respectively equal to $\Delta x = 0.001$ m and $\Delta t = 1$ s.

3. Results and discussion

3.1. Characterization of BWD

The complex materials and properties of brake system components, combined with their exposure to high-energy conditions during braking (which can alter the original structure and chemistry of the resulting wear particles) make precise physical and chemical characterization of brake wear dust inherently challenging. Additionally, associated with BWD properly called, traces of resuspended road material and tire wear, along with unknown bulk frictional materials and uncontrolled driving patterns, are likely to be present. Since the primary aim of this study is to examine the transport behavior of BWD in a saturated porous medium that mimics an aquifer system, the chemical and dimensional characterization serves as a crucial starting point for evaluating the main hazardous components and their dimensions, which could pose environmental risks. In this section, the main results from SEM/EDS, Raman spectroscopy, and ICP-MS analyses are reported and discussed.

3.1.1. SEM/EDX

Electron microscopy analysis of BWD allowed a direct comparison between the morphology (size and shape) and chemical composition of the sample. The particles showed a highly heterogeneous morphology (Fig. 2), characterized by the predominance of fine particles associated with the presence of some coarse irregular ones, which sometimes occur in the form of aggregates. Previous studies suggest that coarse irregular particles usually form as a result of abrasion and fatigue wear of brake components [43]. Angular pieces with sharp edges are less frequent. The predominant fine particles, most likely generated by thermal and/or chemical processes [13,44], showed a quite widespread trend of agglomeration/aggregation to form larger clusters. Despite the heterogeneity in morphology, a common characteristic of fine particles is their tendency to have fewer sharp edges and an almost spherical geometry. Single, non-agglomerated, particles are rare and very small.

The results of dimensional analysis, performed on SEM images using the software ImageJ, were used to create a number size distribution curve, available in Supporting Information (Figure S 3). The d_{50} and d_{90} resulted equal to 0.7 and 3.35 μm , respectively, with a peak at 0.55 μm . Consequently, the BWD characterized in this study represents a

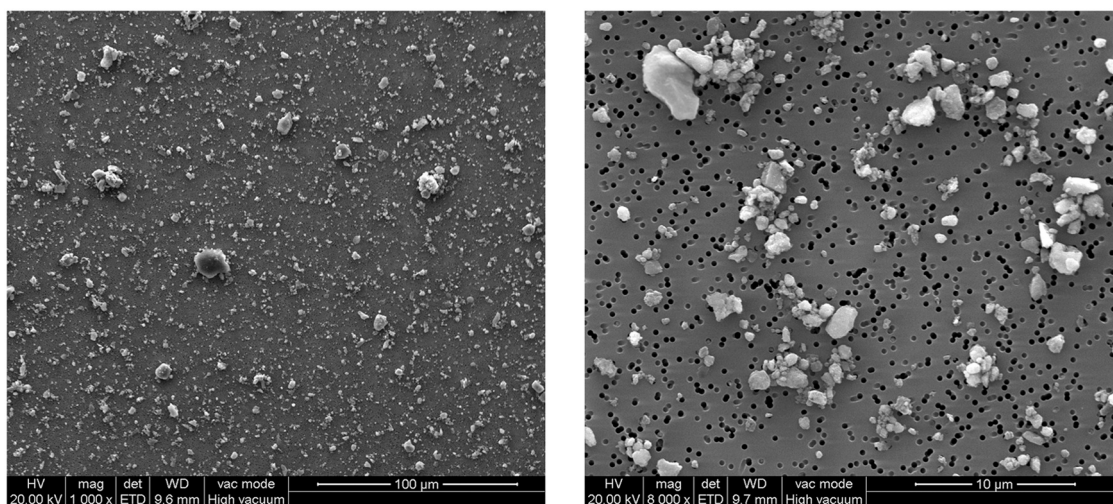


Fig. 2. SEM images of water suspended BWD dried on polycarbonate membrane at (a) 100 μm and (b) 10 μm magnification.

prominent source of $PM_{2.5}$ for the atmospheric domain and a potential risk for subsurface environments when reached. These results are consistent with the previous study of Iijima et al. [45], who found an unimodal number distribution of airborne brake wear particles, with peaks in the range 0.8–1 μm.

The elemental composition from EDX analysis (Figure S 4 and Table S 2) performed over 5 images, for a total of 15 spectra, revealed that Fe was predominant ($35.5\% \pm 17.8\%$), followed by oxygen ($27.3\% \pm 3.0\%$), carbon ($33.7\% \pm 20.6\%$) and silica ($2\% \pm 2.5\%$). Other elements were found at contents lower than 2% (Cu, Mg, Al and Ba). All detected elements are present in the constituents of pads and discs [43] and have been widely associated in the literature with brake wear [46,13,47,45,9,23]. The predominance of Fe among metals may result from abrasion of the disc, which is mostly made of cast iron [16]. Additionally, low metallic (LM) and semi metallic (SM) brake pads wear could represent a source of Fe particles, especially in oxidized form [1, 44]. Carbon is expected to be present in brake wear particles because of the use of graphite as a friction modifier, in addition to the organic resins used as adhesive [43]. In general, most of the particles had Fe- and O-rich compositions, with variable C. In some cases, Si and O were the main components; in those cases, contamination of the original BWD could be attributed to the resuspended soil/road dust, as justified by the BWD sampling procedure adopted in this study. In general, the particles were found very heterogenous in terms of size, shape and composition, as evidenced by the high standard deviation of EDX analysis.

3.1.2. Raman

Raman analysis results are summarized in the pie chart in Fig. 3, illustrating the chemical composition of BWD. The details on the data processing are provided in the Supporting Information. The analysis confirmed the presence of iron compounds as main indicator of BWD, especially in its oxidized form (i.e., hematite and goethite). These results support previous findings in the literature, which showed that the contact surface between the brake pad and the disc is covered by a third body, mainly composed of iron oxides, that can be released as debris during and after braking actions [13,17]. Moreover, several studies report that Fe oxides/hydroxides are abundant in brake pads exposed to air and humidity over long periods [3].

Magnesium oxide, used as material for brake lining fillers, reacts with iron oxide to form magnesioferrite ($MgFe_2O_4$). Iron sulphide may be associated with the presence of iron sulphides-coated steel fibres in the brake pad, which have shown improved stability to withstand the temperature at the pad-disc interface [48]. Graphite is used as a lubricant to reduce noise and enhance friction stability: its presence in BWD was confirmed by Raman analysis, in accordance with Peikertová et al.

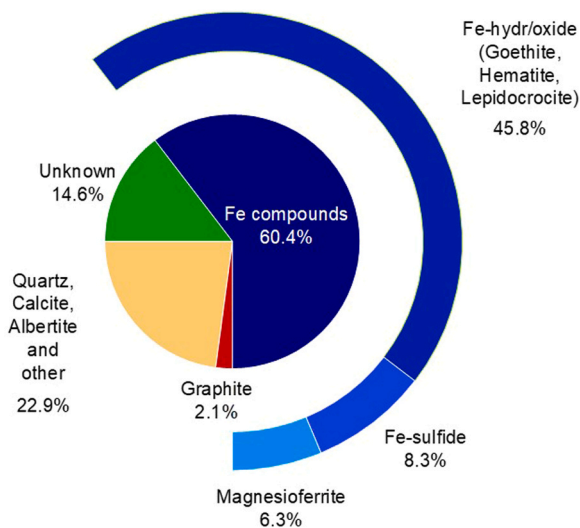


Fig. 3. Chemical composition of BWD derived from the analysis of Raman spectra.

[49]. Conversely, the presence of other phases in wear debris like quartz, calcite and albertite must be attributed to road dust contamination [50].

3.1.3. ICP MS

The metal content of BWD was characterized using ICP-MS. Twenty-three metals were detected, with Fe (90.58%), Cu (3.93%) and Zn (2.28%) being most abundant, which aligns with findings by most researchers in the brake lining. The remaining 3% consists of other secondary metallic elements. A complete characterization of the metals in

Table 1

Results of inductively coupled plasma mass spectrometry (ICP-MS) analysis of BWD metals.

Element	mg/kg	Element	mg/kg	Element	mg/kg
Al	2500	Cr	880	Se	5
Sb	5	Fe	346000	Sn	2900
As	31	Mn	1700	Tl	1
Ba	3500	Hg	0.55	Te	5
Be	5	Mo	230	Ti	150
B	12	Ni	260	V	38
Cd	1	Pb	38	Zn	8700
Co	27	Cu	15000		

BWD is reported in Table 1.

3.2. Column transport tests in saturated conditions

Fig. 4 reports the first part of the BTCs of BWD particles injected in saturated conditions, including particle injection and the first flushing. The complete experimental BTCs, including the second flushing and the NaOH flushing periods, are illustrated in SI (Figure S 5). The preliminary column equilibration is omitted in all graphs. BTCs are plotted as normalized concentration (c/c_0) as a function of PV under different

experimental conditions of water composition and flow velocity.

The column experiments exhibited relatively standard colloid transport behaviour: the breakthrough of the BWD particles reached a steady state plateau during the injection phase, with an outlet concentration (c) always lower than the inflow suspension concentration (c_0). The shape of the breakthrough curves, and in particular the plateau at c/c_0 values much lower than one, suggests that the main retention process is the mechanical filtration of aggregated brake wear particles. Mechanical filtration is often assumed to be an irreversible mechanism, which excludes the potential remobilization of particles by changing the

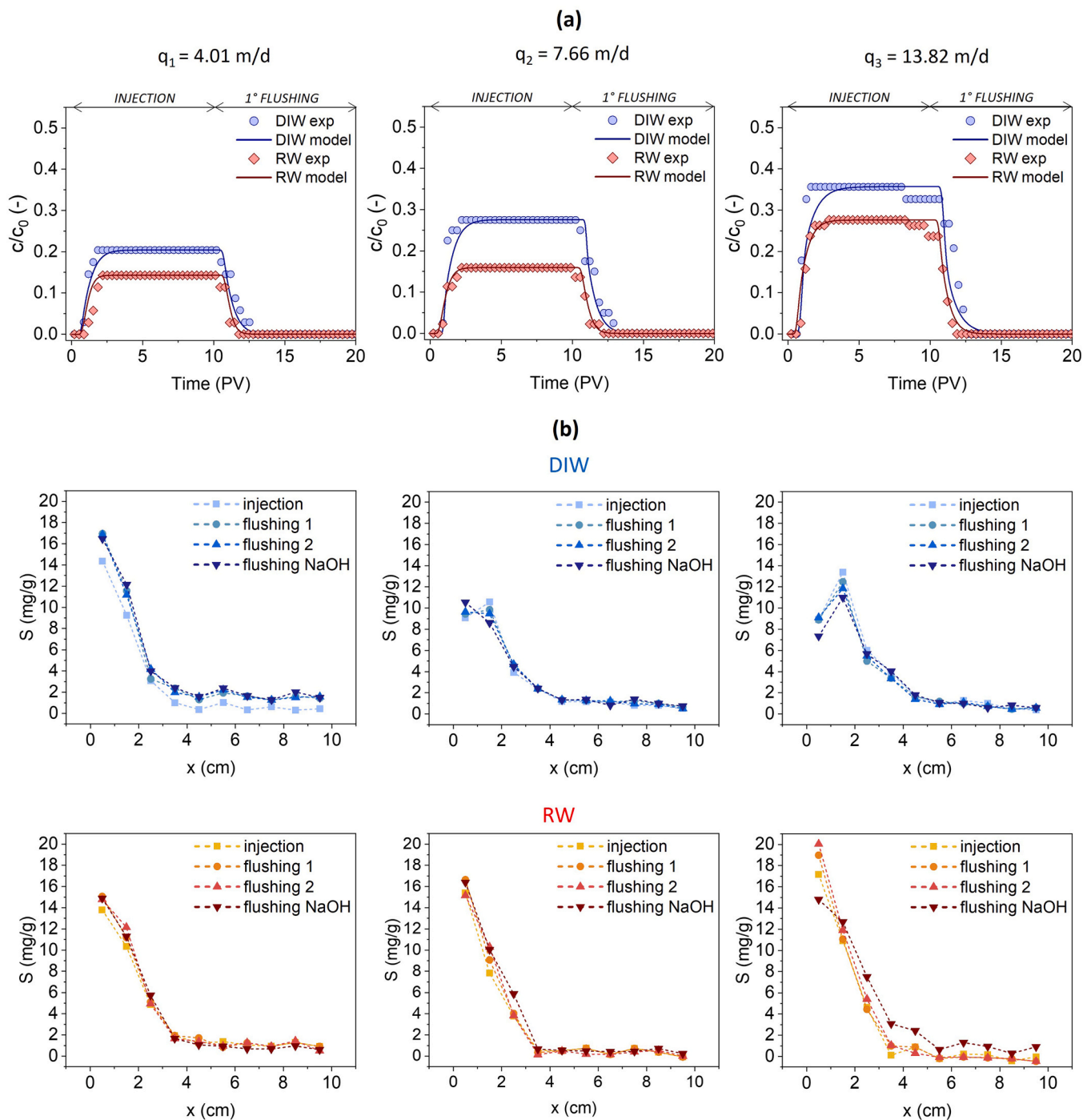


Fig. 4. (a) Breakthrough curves (BTCs) of column transport tests reported as normalized concentration C/C_0 as a function of the number of injected pore volumes (PVs), at different flow velocities ($q_1 < q_2 < q_3$). Experimental data (point values) and modelled curves (lines) are illustrated in blue when BWD is suspended in DIW, in red when BWD is suspended in RW. (b) Experimental spatial profiles (SPs) reported as mass of deposited particles per unit mass of sand (mg/g) at the end of each stress period, for BWD suspended in DIW (first row) or in RW (second row), according to the flow velocities ($q_1 < q_2 < q_3$).

water chemistry. However, the breakthrough curves show an evident tailing during the flushing, suggesting the concurrent reversible deposition of particles following physical-chemical particle-collector interactions [51,52]. This agrees with the observed release peak of deposited particles following changes in water chemistry (Figure S 5), in particular after injection of NaOH, which is expected to increase repulsion among particles (thus partly breaking aggregates) and between particles and sand grains (thus promoting release).

Under water-saturated conditions, the BWD effluent concentrations progressively increased with increasing flow rate. At the slowest Darcy velocity of 4.01 m/d (q_1), BWD effluent concentrations reached a maximum relative concentration of nearly 0.20 when pore water was DIW, and 0.13 in RW. At higher pore water velocities of 7.66 and 13.82 m/d, greater breakthrough was achieved, with effluent concentrations reaching 26 % (DIW) and 17.05 % (RW) of the influent concentration for $q_2 = 7.66$ m/d, and 35.64 % (DIW) and 26.53 % (RW) of the influent concentration for $q_3 = 13.82$ m/d. Fig. 4 also shows that under the same flow velocity, deposition phenomena inside the column are favoured by RW as dispersing solution, since the higher ionic strength acts to screen repulsive electrostatic forces, in accordance with DLVO theory [53-55].

All retention profiles (Fig. 4 (b)) exhibited a hyper-exponential shape. For tests conducted using DIW as dispersant fluid (Fig. 4 (b) – first row), increasing the flow rate resulted in more limited BWD deposition, especially in the first centimeters of the column. For the intermediate and highest flow rates, which resulted in evident release peaks following NaOH injection (Figure S 5), the profiles also show that flushing with NaOH promoted the detachment predominantly in the first centimeters of the column, where most particles were retained, with minimal release at longer distances and no evident re-location of the particles along the column. In contrast, experiments conducted using RW (Fig. 4 (b) – second row) showed a different behaviour: even if the mass balances (Table 2) and breakthrough curves indicate that less particles are retained at higher velocity, similarly to tests conducted in DIW, for particles dispersed in RW increasing flow velocity resulted in a greater mass of brake wear dust deposited in the first few centimetres of the column, with consequently steeper profiles. Flushing with NaOH resulted, particularly for the highest velocity, in both a (limited) release of deposited particles (as indicated by breakthrough curves, see Figure S 5) and their re-location along the column.

The part of the breakthrough curves corresponding to the BWD injection and the first flushing were modelled using equations (3) and (4) using the software MNMs 2021 as described in the Methods section. Two concurrent interaction sites were used, namely site 1 (linear irreversible deposition) modelling mechanical filtration, and site 2 (linear reversible deposition) modelling physical-chemical attachment. The agreement between the fitted and experimental curves (Fig. 4 (a)) is good in all cases, as evidenced also by the coefficients of determination R^2 always higher than 0.95, and confirms the accuracy with which kinetic rates, presented in Table 3, could be estimated. All deposition and release

Table 2

Column transport tests in saturated conditions: mass balances after injection, first and second flushing, and NaOH flushing, reported according to the flow velocity and the dispersing water used for each test. Comparison (relative change) between deposition percentage resulting from BTCs ($M_{INJ}-M_{BTC}$) and SPs (M_{DEP}) analysis.

Stress period	Pore water	q_1			q_2			q_3		
		$M_{INJ}-M_{BTC}$ (%)	M_{DEP} (%)	Relative change (%)	$M_{INJ}-M_{BTC}$ (%)	M_{DEP} (%)	Relative change (%)	$M_{INJ}-M_{BTC}$ (%)	M_{DEP} (%)	Relative change (%)
After inj.	DI	81.48	60.63	25.59	78.22	64.79	17.17	69.41	67.41	2.88
	RW	89.33	77.40	13.35	86.59	51.84	40.13	77.59	49.54	36.15
After 1 ^o flush.	DI	79.91	86.75	8.57	74.59	67.74	9.18	63.07	63.03	0.06
	RW	86.95	82.23	5.43	84.62	56.12	33.68	74.61	52.16	30.09
After 2 ^o flush.	DI	79.91	88.08	10.22	74.59	66.91	10.29	63.07	62.72	0.56
	RW	86.86	81.57	6.09	84.62	53.76	36.47	74.35	56.04	24.62
After NaOH flush.	DI	79.72	91.44	14.7	74.00	66.93	9.55	61.49	60.47	1.66
	RW	86.67	78.48	9.45	82.95	61.79	25.51	73.47	69.95	4.80

Table 3

Column transport tests in saturated conditions: fitted attachment/detachment coefficients ($k_{a,1}$, $k_{a,2}$ and $k_{d,2}$), porosity (n), dispersivity in saturated conditions (α_{sat}) and coefficient of determination R^2 of the two-site transport model for different pore water velocities ($q_1 < q_2 < q_3$) and pore water (DIW, RW).

Parameter	q_1		q_2		q_3	
	DIW	RW	DIW	RW	DIW	RW
Site 1 $k_{a,1}$ (s^{-1})	$2.0 \cdot 10^{-3}$	$2.4 \cdot 10^{-3}$	$2.9 \cdot 10^{-3}$	$3.9 \cdot 10^{-3}$	$3.7 \cdot 10^{-3}$	$4.3 \cdot 10^{-3}$
Site 2 $k_{a,2}$ (s^{-1})	$1.4 \cdot 10^{-3}$	$2.7 \cdot 10^{-4}$	$2.0 \cdot 10^{-3}$	$7.7 \cdot 10^{-4}$	$3.0 \cdot 10^{-3}$	$8.0 \cdot 10^{-4}$
$k_{d,2}$ (s^{-1})	$3.3 \cdot 10^{-3}$	$2.2 \cdot 10^{-3}$	$5.0 \cdot 10^{-3}$	$3.7 \cdot 10^{-3}$	$6.1 \cdot 10^{-3}$	$4.3 \cdot 10^{-3}$
n (-)	0.37	0.38	0.39	0.43	0.4	0.48
α_{sat} (m)	$1.7 \cdot 10^{-3}$	$1.3 \cdot 10^{-3}$	$1.0 \cdot 10^{-3}$	$1.3 \cdot 10^{-3}$	$1.0 \cdot 10^{-3}$	$1.7 \cdot 10^{-3}$
R^2 (-)	0.99	0.96	0.98	0.99	0.97	0.99

kinetics clearly depend on both ionic strength and flow rate. An increase in both attachment and detachment rates with the Darcy velocity was observed regardless of pore water chemistry, coherently with the literature [56,57]. At the same flow velocity, a higher ionic strength (RW) resulted in higher values of $k_{a,1}$, indicating a more pronounced mechanical filtration in RW likely associated to more aggregated BWD. The reversible attachment and detachment rates, $k_{a,2}$ and $k_{d,2}$, are both lower in RW compared to DIW, suggesting a lower impact of physical-chemical phenomena compared to mechanical filtration in this set of tests.

3.3. Column transport tests in unsaturated conditions

Fig. 5 shows the BTCs of the two tests performed injected BWD suspensions in sand-packed partially saturated columns. The experimental data of the overall BTCs are reported in Figure S 6 in SI.

The shape of the BTCs was very similar to those obtained under saturated conditions, showing, also in this case, the predominance of the mechanical filtration phenomenon. At lower pore water velocity (q_1), lower breakthrough was achieved, with effluent concentrations reaching 30 % of the influent concentration. When the flow velocity was the highest tested (q_3), the plateau value of the BTC reached 0.44. An asymmetry between the rise and fall of dimensionless concentration over time is observed. The smoother tail indicates a detachment of particles weakly deposited on the porous medium surface.

Compared to the respective saturated conditions test, under the same injection flow rate and mass of BWD, the lower saturation leads to greater contaminant mobility in the same porous medium. It is known from the literature that several mechanisms collectively contribute to the observed behavior whereby particles may move more effectively in unsaturated media compared to fully saturated media: under unsaturated conditions, where grains are surrounded by a thin film of water, colloidal particles are often immobilized by capillary forces, but, as the water films expand or move through the porous medium, these same capillary forces can facilitate the detachment and transport of particles along with the shifting liquid-gas interfaces [58].

The spatial profiles of the BWD mass deposited per unit mass of the

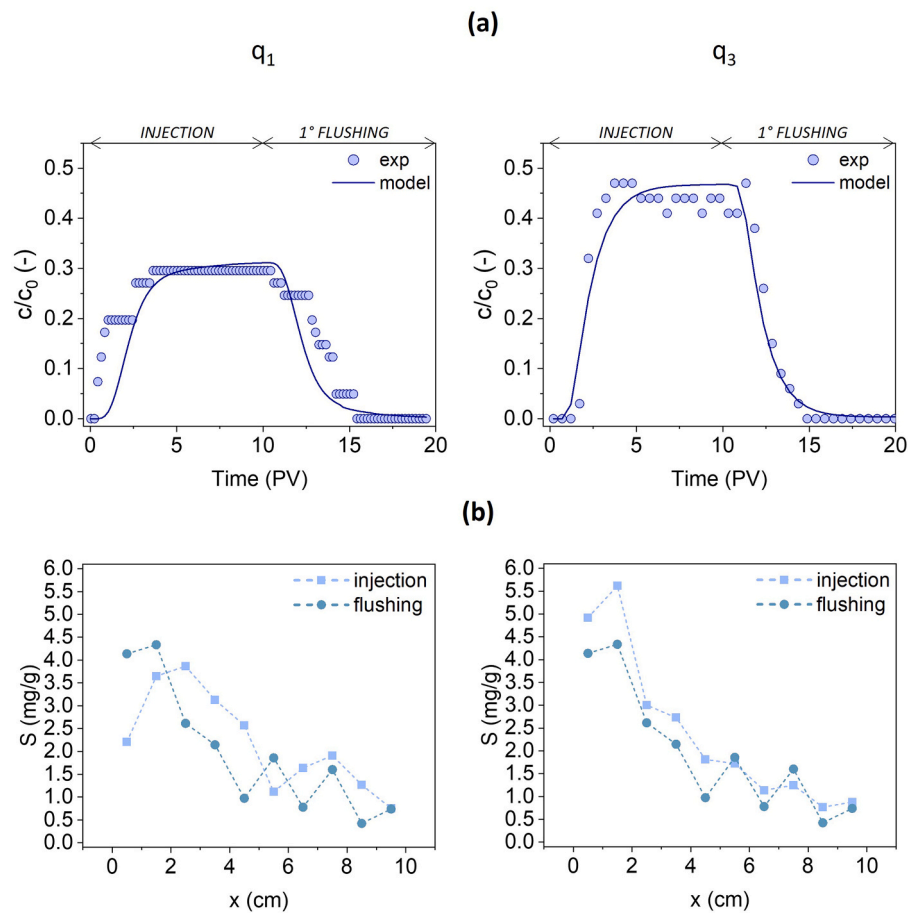


Fig. 5. Unsaturated tests in sand: (a) Breakthrough curves (BTCs) of column transport tests reported as normalized concentration c/c_0 as a function of the number of pore volumes injected, divided in two graphs according to the corresponding flow velocities ($q_1 < q_3$). The experimental data are shown as points, and the modelled curves as lines. (b) Experimental spatial profiles (SPs) reported as deposited particles per unit mass of sand (mg/g) along the columns at the end of each stress period, according to the flow velocities ($q_1 < q_3$).

porous medium are shown in Fig. 5 (b). The profiles showed a decline along the columns, which was more pronounced at higher flow rate. Moreover, the impact of the flushing on the retained concentrations is more pronounced compared to saturated tests: in unsaturated conditions, after flushing the concentration profile lowers and is partly shifted toward larger distances from the column inlet, as a consequence of a partial BWD release (as evident in the tailing of the breakthrough curve) and re-location in the column. The mass balances (Table 4) coherently show a decline in the retained BWD mass with flushing steps.

Two standard soils (LUFA 2.2 and LUFA 2.4) were finally tested for BWD transport under unsaturated conditions, at the highest flow velocity q_3 , mimicking the possible behaviour of the particles in top-soils (Fig. 6). The experimental data of the overall BTCs are reported in Figure S 6 in SI. In the sandy soil (LUFA 2.2), particle mobility is still evident, albeit reduced compared to sand at the same flow rate. Conversely, in the clayey loam (LUFA 2.4), a complete deposition of

BWD particles is observed, resulting in no breakthrough during the test. The soil LUFA 2.4 is characterized by a fine texture and high clay content. The fine pores in clayey loam soils can physically trap larger particles and aggregates, preventing their movement through the soil matrix. Moreover, clayey loam soils have a large specific surface area and a high cation exchange capacity (CEC), both of which can contribute to the strong retention of finer particles. Consequently, spatial profiles showed a hyper-exponential shape, with high particle concentrations particularly within the initial centimetres of the column (Fig. 6(b)). In general, the shape of the spatial deposition profiles is consistent with strong mechanical filtration, especially in the first section of the porous medium. This behavior is valid for both soils, and the results obtained complement the BTCs. Moreover, in these tests no evident release of particles was promoted during flushing, as evidenced by the almost unaltered concentration profiles at the end of injection and after the two flushing steps and confirmed by mass balances (Table 4). This finding

Table 4

Column transport tests in saturated conditions: mass balances after injection, first and second flushing, reported according to the flow velocity and the porous medium used for each test. Comparison (relative change) between deposition percentage resulting from BTCs ($M_{INJ-M_{BTC}}$) and SPs (M_{DEP}) analysis.

Stress period	q_1 Dorsilit 8			q_3 Dorsilit 8			q_3 LUFA 2.2			q_3 LUFA 2.4		
	$M_{INJ-M_{BTC}}$ (%)	M_{DEP} (%)	Rel. change (%)	$M_{INJ-M_{BTC}}$ (%)	M_{DEP} (%)	Rel. change (%)	$M_{INJ-M_{BTC}}$ (%)	M_{DEP} (%)	Rel. change (%)	$M_{INJ-M_{BTC}}$ (%)	M_{DEP} (%)	Rel. change (%)
After inj.	75.06	51.26	31.71	64.91	73.5	13.23	83.73	57.10	31.80	99.73	57.16	42.69
After 1° flush.	63.43	38.62	39.12	56.1	60.39	7.64	82.35	56.51	31.38	99.73	59.42	40.42
After 2° flush.				55.27	53.91	2.45	82.16	57.22	30.35	99.73	60.86	38.98

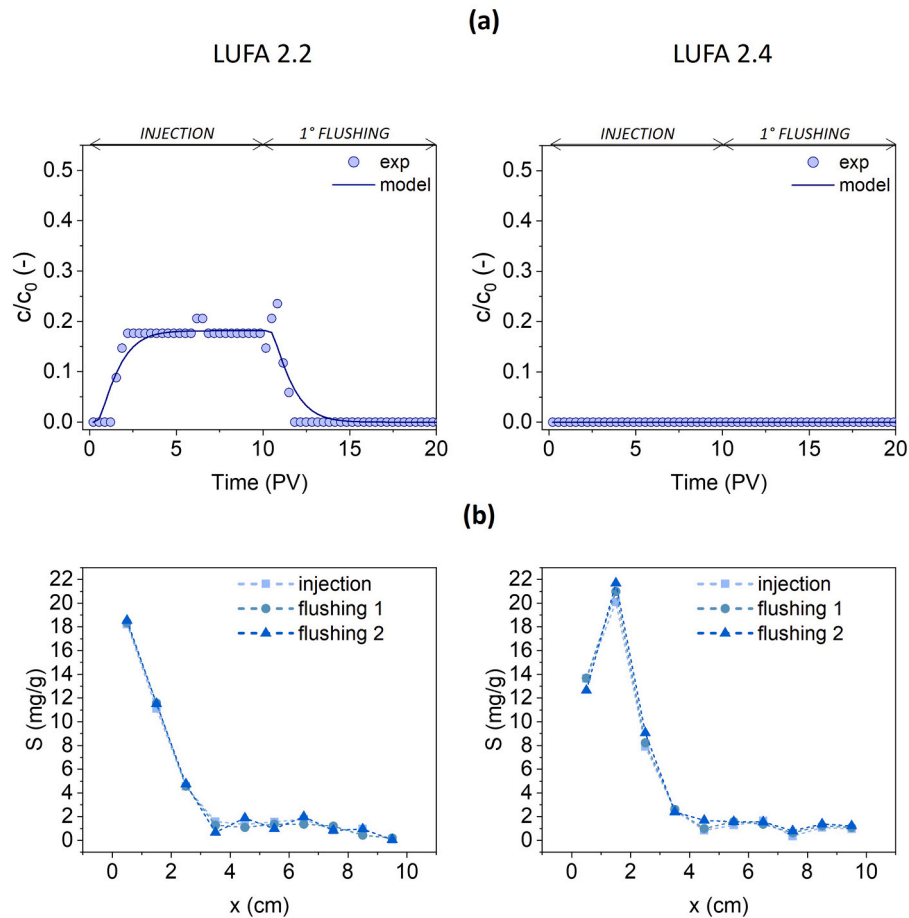


Fig. 6. Unsaturated tests in soils: (a) Breakthrough curves (BTCs) of column transport tests reported as normalized concentration c/c_0 as a function of the number of pore volumes injected, divided in two graphs according to the corresponding flow velocities (q_1 and q_3). The experimental data are shown as points, and the modelled curves as lines. (b) Experimental spatial profiles (SPs) reported as deposited particles per unit mass of soil (mg/g) along the columns at the end of each stress period, according to the flow velocities ($q_1 < q_3$).

suggests a minor contribution of reversible physical-chemical attachment to particle retention in the column, contrary to the tests performed in sand-packed unsaturated columns, where the lowering of the concentration profiles with column flushing was symptomatic of a non-negligible reversible attachment.

Similarly to saturated column tests, also for unsaturated tests the experimental BTCs were modelled to equations (3) and (4) considering a linear irreversible and a linear reversible retention mechanisms (Table 5). The fitting was satisfactory in all cases, with coefficients of

Table 5

Column transport tests in unsaturated conditions: fitted attachment/detachment coefficients ($k_{a,1}$, $k_{a,2}$ and $k_{d,2}$), porosity (n), dispersivity in saturated and unsaturated conditions (α_{sat} and α_{unsat} , respectively), water content (θ) and coefficient of determination R^2 of the two-site transport model for different pore water velocities (q_1 and q_3) and porous media (Dorsilit 8, LUFA 2.2 and LUFA 2.4).

Parameter	q_1		q_3	
	Dorsilit 8	Dorsilit 8	LUFA 2.2	LUFA 2.4
Site 1 $k_{a,1}$ (s^{-1})	$1.36 \cdot 10^{-3}$	$3.33 \cdot 10^{-3}$	$7.24 \cdot 10^{-3}$	nd
Site 2 $k_{a,2}$ (s^{-1})	$1.8 \cdot 10^{-3}$	$3.5 \cdot 10^{-3}$	$8.59 \cdot 10^{-3}$	nd
$k_{d,2}$ (s^{-1})	$1.4 \cdot 10^{-3}$	$7.0 \cdot 10^{-3}$	$1.0 \cdot 10^{-2}$	nd
n (-)	0.37	0.38	0.35	0.39
α_{unsat} (m)	$6.1 \cdot 10^{-3}$	$4.1 \cdot 10^{-3}$	$7 \cdot 10^{-3}$	$1.0 \cdot 10^{-2}$
α_{sat} (m)	$1.7 \cdot 10^{-3}$	$1.0 \cdot 10^{-3}$	$3.5 \cdot 10^{-4}$	$6.5 \cdot 10^{-4}$
θ (-)	0.28	0.28	0.3	0.32
R^2 (-)	0.91	0.93	0.94	nd

determination R^2 always higher than 0.90.

The attachment and detachment coefficients increase with velocity, as previously observed for saturated tests. The fitting parameters obtained for tests under partial saturation in sand are of the same order of magnitude as those obtained for saturated tests. Specifically, the attachment coefficient for the irreversible site ($k_{a,1}$) is higher in saturated conditions compared to unsaturated conditions at both flow rates, coherently with the lower plateau observed in the breakthrough curves for saturated conditions compared to unsaturated ones. The higher particle retention in LUFA 2.2 soil compared to sand, at the same velocity, results in higher values for the attachment and detachment coefficients.

The modelling work evidences the importance of incorporating both irreversible and reversible retention mechanisms to accurately predict particle behaviour in unsaturated media. This approach helps capture the complex interplay of factors that govern contaminant transport, highlighting the necessity for detailed soil characterization when assessing environmental risks. Future research should focus on refining these models and exploring the implications of these findings across a broader range of soil types and environmental conditions.

3.4. Implications for field-scale conditions

The results of the column transport tests herein presented provide useful insights into the potential key factors and mechanisms controlling BWD mobility in soils and groundwater also at field scale. Even if the results obtained in laboratory-scale transport tests cannot be directly up-

scaled to the field in quantitative terms without a validation with field data, this study aims at setting a first step in the understanding of the key mechanisms controlling the transport in porous media of BWD, paving the way for further investigations at larger scales.

It is evident from the laboratory results that the soil can act as a filter toward the leaching of BWD into the subsoil. On the one hand, soil composition and texture play a critical role in particle retention: clay-rich soils can exhibit almost complete particle deposition, significantly contributing to limit BWD leaching to deeper soils and ultimately groundwater. On the other hand, BWD can move more readily and have a greater transport capacity in coarser unsaturated soils compared to the saturated zone, which they may reach and continue to migrate: the vadose zone may serve as a region where the BWD demonstrates considerable mobility, thus posing possible environmental risks. Understanding the potential for BWD leaching in these environments is vital, especially to identify the scenarios where soil filtration mechanisms might fully capture BWD particles, and those in which this is not possible. All in all, the presented laboratory results substantiate the feasibility of contaminant migration from the ground surface to the fully saturated zone, attributable to the enhanced mobility within the unsaturated subsurface. However, additional investigations are still needed to further determine the mechanisms governing the deposition and transport of BWD particles in unsaturated sand.

The role of the top-soil as a filter has a duplex environmental implication: fine soils can prevent groundwater pollution, retaining most particulate emitted by road traffic, but this phenomenon can lead to the accumulation of such particles in the soils in vicinity to roads and in urban area. This aspect is critical for non-exhaust emissions due to their content in heavy metals, as already evidenced by previous literature studies.

Finally, it is worth highlighting that the substantial absence of regulations by governmental agencies on estimation, characterization and limitation of brake wear dust emissions further contributes to making them an environmental concern. The upcoming Euro 7 standards will introduce specific limits for brake and tire particulate emissions, based on the Global Technical Regulation 24 (GTR 24) [59]. In particular, Euro 7 emission regulation sets a limit for brake non-exhaust PM10 emissions at 7 mg/km per vehicle during standard driving cycles. This limit will remain in place until December 31, 2034, and will be reduced to 3 mg/km per vehicle starting January 1, 2035 [60]. GTR 24 also sets standardized procedures for measuring brake emissions in light-duty vehicles, utilizing brake dynamometers under the WLTP-Brake test cycle [61]. In contrast, tire particulate emissions pose an additional challenge due to their strong dependence on road surface interaction, leading to considerable variability in emission factors even under comparable driving conditions. The need of establishing standard methodologies to verify and limit such emissions has been evidenced by the literature in terms of air pollution, and this work aims at evidencing its relevance also in terms of groundwater quality protection.

4. Conclusions

Numerous research studies have already confirmed braking of cars to be a potential source of both airborne and non-airborne particulate emissions because each forced deceleration through friction brake releases wear particles. Conversely, a challenging and almost neglected area in the field of non-exhaust emissions is the understanding of the potential impact of BWD on the subsurface environment. The fate of brake wear particles, once emitted in subsoil, is almost not known yet. This study for the first time investigates the transport mechanisms of BWD, modified with humic acids commonly present in the subsoil, in saturated porous media mimicking sandy aquifers and unsaturated porous media mimicking the top-soil and unsaturated zone.

Our results show that HA-coated brake wear particles can be mobile in the subsoil, since they exhibit non-negligible transport in laboratory column tests. In particular, the experiments highlighted the crucial role

of the soil as first filter against leaching of BWD particles in the unsaturated zone and in groundwater.

Our experimental results also suggest that BWD transport in both silica sand and in real soils is affected by the physical-chemical interactions with the solid matrix (in turn influenced by ionic strength of the dispersing water) and by mechanical filtration, thus implying that if, on the one hand, larger particles may be retained by the soil, finer particles may migrate and leach toward groundwater following rain events. Moreover, changes in water geochemistry, e.g. pH increase, can lead to remobilization of already deposited particles.

Research on the environmental behavior of BWD in porous media, such as natural soils, remains crucial due to the potential environmental impact of these particles. Continuation of these studies is necessary, particularly to understand the dynamics of BWD mobility in unsaturated porous media, reproducing as close as possible the conditions found in the top-soils and in the vadose zone.

Moreover, a key area for future research is the role of BWD as a carrier for other pollutants. Given the high iron oxide content in brake wear dust and its well-documented adsorption capacity, BWD could potentially transport other hazardous substances through porous media. This could exacerbate the environmental impact, as pollutants bound to BWD particles may be more mobile and persistent, leading to broader contamination of soil and water systems. Understanding how BWD interacts with different soil types, moisture levels, and other environmental factors is essential for predicting and mitigating the long-term environmental risks associated with these particles, both as contaminant themselves and as potential carriers of other molecules.

In conclusion, a comprehensive understanding of BWD in both saturated and unsaturated porous media is critical for developing effective strategies to manage its environmental fate. This work establishes a first step in the understanding of the key phenomena controlling subsurface mobility of BWD. By focusing on the interplay between BWD and other pollutants, as well as the mechanisms of leaching and transport in different soil types, researchers can better predict the behavior of these particles and propose measures to protect soil and water resources from contamination.

Environmental implication

Brake wear dust (BWD) is a major non-exhaust emission (NEE) in urban areas, accounting for 16–55 % of road traffic PM10. The increasing adoption of heavier electric vehicles exacerbates BWD emissions, despite reductions in exhaust pollutants. BWD particles, generated through frictional wear of brake pads and rotors, are chemically diverse and can act as carriers for other contaminants, posing risks to soil and water systems. However, the environmental fate and transport of BWD remain poorly understood, creating a critical knowledge gap. Addressing this gap is essential for evaluating its potential negative effects on urban ecosystems and developing effective mitigation strategies.

Funding

Part of the research reported in this paper received financial support has received funding in the framework of the project RETURN from the MUR - I1.3-PE00000005 – CUP I33C22006910006 of PNRR funded by the European Union – NextGenerationEU.

CRedit authorship contribution statement

Bianco Carlo: Writing – review & editing, Software, Methodology. **Acocella Michela:** Writing – review & editing, Writing – original draft, Validation, Methodology, Investigation, Data curation. **Sethi Rajandrea:** Writing – review & editing, Supervision, Software, Methodology, Funding acquisition, Formal analysis, Conceptualization. **Tosco Tiziana:** Writing – review & editing, Supervision, Software, Methodology,

Formal analysis, Data curation, Conceptualization.

Declaration of Competing Interest

The authors declare that they have no known competing financial interests or personal relationships that could have appeared to influence the work reported in this paper.

Acknowledgments

The authors thank Amelia Piscitello for the contribution to the initial planning and design of the experiments.

Appendix A. Supporting information

Supplementary data associated with this article can be found in the online version at [doi:10.1016/j.jhazmat.2025.137851](https://doi.org/10.1016/j.jhazmat.2025.137851).

Data availability

Data will be made available on request.

References

- Piscitello, A., Bianco, C., Casasso, A., Sethi, R., 2021. Non-exhaust traffic emissions: sources, characterization, and mitigation measures. *Sci Total Environ* 766, 144440. <https://doi.org/10.1016/j.scitotenv.2020.144440>.
- World Health Organization. (2023). World health statistics. In World health statistics 2023: monitoring health for the SDGs, Sustainable Development Goals. <https://doi.org/10.2307/3348165>.
- Pellecchia, M., Papa, G., Barbato, M., Capitani, G., Negri, I., 2023. Origin of non-exhaust PM in cities by individual analysis of particles collected by honey bees (*Apis mellifera*). *Environ Pollut* 331 (August 2022), 121885. <https://doi.org/10.1016/j.envpol.2023.121885>.
- Richter, J.L., 2022. A circular economy approach is needed for electric vehicles. *Nat Electron* 5 (1), 5–7. <https://doi.org/10.1038/s41928-021-00711-9>.
- Hooftman, N., Messagie, M., Joint, F., Segard, J.B., Coosemans, T., 2018. In-life range modularity for electric vehicles: The environmental impact of a range-extender trailer system. *Appl Sci (Switz)* 8 (7). <https://doi.org/10.3390/app8071016>.
- Liu, Y., Chen, H., Li, Y., Gao, J., Dave, K., Chen, J., et al., 2022. Exhaust and non-exhaust emissions from conventional and electric vehicles: a comparison of monetary impact values. *J Clean Prod* 331 (December 2021), 129965. <https://doi.org/10.1016/j.jclepro.2021.129965>.
- McCarty, K., Mian, H.R., Chhipi-Shrestha, G., Hewage, K., Sadiq, R., 2023. Ecological risk assessment of tire and road wear particles: a preliminary screening for freshwater sources in Canada. *Environ Pollut* 325 (December 2022), 121354. <https://doi.org/10.1016/j.envpol.2023.121354>.
- Liu, Y., Chen, H., Gao, J., Li, Y., Dave, K., Chen, J., et al., 2021. Comparative analysis of non-exhaust airborne particles from electric and internal combustion engine vehicles. *J Hazard Mater* 420, 126626. <https://doi.org/10.1016/j.jhazmat.2021.126626>.
- Iijima, A., Sato, K., Yano, K., Tago, H., Kato, M., Kimura, H., et al., 2007. Particle size and composition distribution analysis of automotive brake abrasion dusts for the evaluation of antimony sources of airborne particulate matter. *Atmos Environ* 41 (23), 4908–4919. <https://doi.org/10.1016/j.atmosenv.2007.02.005>.
- OECD, 2020. Non-exhaust Particulate Emissions from Road Transport An Ignored Environmental Policy Challenge. Non-Exhaust Particulate Emissions from Road Transport An Ignored Environmental Policy Challenge, 2030, p. 149. (<https://www.proquest.com/books/non-exhaust-particulate-emissions-road-transport/docview/2690236533/se-2?accountid=206735>).
- Amato, F., Cassee, F.R., Denier van der Gon, H.A.C., Gehrig, R., Gustafsson, M., Hafner, W., et al., 2014. Urban air quality: the challenge of traffic non-exhaust emissions. *J Hazard Mater* 275, 31–36. <https://doi.org/10.1016/j.jhazmat.2014.04.053>.
- Denby, B.R., Sundvor, I., Johansson, C., Pirjola, L., Ketzler, M., Norman, M., et al., 2013. A coupled road dust and surface moisture model to predict non-exhaust road traffic induced particle emissions (NORTRIP). Part 1: road dust loading and suspension modelling. *Atmos Environ* 77, 283–300. <https://doi.org/10.1016/j.atmosenv.2013.04.069>.
- Grigoratos, T., Martini, G., 2015. Brake wear particle emissions: a review. *Environ Sci Pollut Res* 22 (4), 2491–2504. <https://doi.org/10.1007/s11356-014-3696-8>.
- Harrison, R.M., Jones, A.M., Gietl, J., Yin, J., Green, D.C., 2012. Estimation of the contributions of brake dust, tire wear, and resuspension to nonexhaust traffic particles derived from atmospheric measurements. *Environ Sci Technol* 46 (12), 6523–6529. <https://doi.org/10.1021/es300894r>.
- Selley, L., Schuster, L., Marbach, H., Forsthuber, T., Forbes, B., Gant, T.W., et al., 2020. Brake dust exposure exacerbates inflammation and transiently compromises phagocytosis in macrophages. *Metallomics* 12 (3), 371–386. <https://doi.org/10.1039/c9mt00253g>.
- Nyirő-Kósa, I., Ahmad, F., Hoffer, A., Pósfai, M., 2022. Nanoscale physical and chemical properties of individual airborne magnetic particles from vehicle emissions. *Atmos Environ: X* 15 (ember 2021). <https://doi.org/10.1016/j.aeoaa.2022.100181>.
- Österle, W., Urban, I., 2006. Third body formation on brake pads and rotors. *Tribology Int* 39 (5), 401–408. <https://doi.org/10.1016/j.triboint.2005.04.021>.
- Sinha, A., Ischia, G., Menapace, C., Gialanella, S., 2020. Experimental characterization protocols for wear products from disc brake materials, 11. <https://doi.org/10.3390/atmos11101102>.
- Kumar, S., Ghosh, S.K., 2020. Particle emission of organic brake pad material: a review. *Proc Inst Mech Eng, Part D: J Automob Eng* 234 (5), 1213–1223. <https://doi.org/10.1177/0954407019879839>.
- rDall'Osto, M., Querol, X., Amato, F., Karanasiou, A., Lucarelli, F., Nava, S., et al., 2013. Hourly elemental concentrations in PM2.5 aerosols sampled simultaneously at urban background and road site during SAPUSS-diurnal variations and PMF receptor modelling. *Atmos Chem Phys* 13 (8), 4375–4392. <https://doi.org/10.5194/acp-13-4375-2013>.
- Gietl, J.K., Lawrence, R., Thorpe, A.J., Harrison, R.M., 2010. Identification of brake wear particles and derivation of a quantitative tracer for brake dust at a major road. *Atmos Environ* 44 (2), 141–146. <https://doi.org/10.1016/j.atmosenv.2009.10.016>.
- Johansson, C., Norman, M., Burman, L., 2009. Road traffic emission factors for heavy metals. *Atmos Environ* 43 (31), 4681–4688. <https://doi.org/10.1016/j.atmosenv.2008.10.024>.
- Liati, A., Schreiber, D., Lugovyy, D., Gramstat, S., Dimopoulos Eggenschwiler, P., 2019. Airborne particulate matter emissions from vehicle brakes in micro- and nano-scales: morphology and chemistry by electron microscopy. *Atmos Environ* 212 (May), 281–289. <https://doi.org/10.1016/j.atmosenv.2019.05.037>.
- Kazimirova, A., Peikertova, P., Barancokova, M., Staruchova, M., Tulinska, J., Vaculik, M., et al., 2016. Automotive airborne brake wear debris nanoparticles and cytokinesis-block micronucleus assay in peripheral blood lymphocytes: a pilot study. *Environ Res* 148, 443–449. <https://doi.org/10.1016/j.envres.2016.04.022>.
- Khalid, N., Hussain, M., Young, H.S., Boyce, B., Aqeel, M., Noman, A., 2018. Effects of road proximity on heavy metal concentrations in soils and common roadside plants in Southern California. *Environ Sci Pollut Res* 25 (35), 35257–35265. <https://doi.org/10.1007/s11356-018-3218-1>.
- Singh, A.K., Choudhary, J.K., Shukla, S.K., Baudhh, K., Pandey, G., Madhav, S., et al., 2025. Agroecosystem contamination with heavy metals due to road transportation: a global threat to safe food security. *Process Saf Environ Prot* 194 (October 2024), 1265–1282. <https://doi.org/10.1016/j.psep.2024.12.046>.
- Wang, M., Zhang, H., 2018. Accumulation of heavy metals in roadside soil in urban area and the related impacting factors. *Int J Environ Res Public Health* 15 (6). <https://doi.org/10.3390/ijerph15061064>.
- Rahimi, M., Bortoluzzi, D., Wahlström, J., 2021. Input parameters for airborne brake wear emission simulations: a comprehensive review. *Atmosphere* 12 (7), 1–26. <https://doi.org/10.3390/atmos12070871>.
- Baensch-Baltruschat, B., Kocher, B., Kochleus, C., Stock, F., Reifferscheid, G., 2021. Tyre and road wear particles - a calculation of generation, transport and release to water and soil with special regard to German roads. *Sci Total Environ* 752, 141939. <https://doi.org/10.1016/j.scitotenv.2020.141939>.
- Baalousha, M., 2009. Aggregation and disaggregation of iron oxide nanoparticles: Influence of particle concentration, pH and natural organic matter. *Sci Total Environ* 407 (6), 2093–2101. <https://doi.org/10.1016/j.scitotenv.2008.11.022>.
- Illés, E., Tombác, E., 2006. The effect of humic acid adsorption on pH-dependent surface charging and aggregation of magnetite nanoparticles. *J Colloid Interface Sci* 295 (1), 115–123. <https://doi.org/10.1016/j.jcis.2005.08.003>.
- Tiraferrri, A., Saldarriaga Hernandez, L.A., Bianco, C., Tosco, T., Sethi, R., 2017. Colloidal behavior of goethite nanoparticles modified with humic acid and implications for aquifer reclamation. *J Nanopart Res* 19 (3). <https://doi.org/10.1007/s11051-017-3814-x>.
- Abramoff, M.D., Magalhães, P.J., Ram, S.J., 2004. Image processing with imageJ. *Biophotonics Int* 11 (7), 36–41. <https://doi.org/10.1201/9781420005615.ax4>.
- Magherini, L., Avataneo, C., Capella, S., Lasagna, M., Bianco, C., Belluso, E., et al., 2023. Mobility of crocidolite asbestos in sandy porous media mimicking aquifer systems. *J Hazard Mater* 458 (June), 131998. <https://doi.org/10.1016/j.jhazmat.2023.131998>.
- Hosseini, S.M., Tosco, T., 2013. Transport and retention of high concentrated nano-Fe/Cu particles through highly flow-rated packed sand column. *Water Res* 47 (1), 326–338. <https://doi.org/10.1016/j.watres.2012.10.002>.
- Bianco, C., Patiño Higuera, J.E., Tosco, T., Tiraferrri, A., Sethi, R., 2017. Controlled deposition of particles in porous media for effective aquifer nanoremediation. *Sci Rep* 7 (1), 1–10. <https://doi.org/10.1038/s41598-017-13423-y>.
- Tosco, T., Sethi, R., 2009. MNMID: a numerical code for colloid transport in porous media: Implementation and validation. *Am J Environ Sci* 5 (4), 516–524. <https://doi.org/10.3844/ajessp.2009.516.524>.
- Dalla Vecchia, E., Luna, M., Sethi, R., 2009. Transport in porous media of highly concentrated iron micro- and nanoparticles in the presence of xanthan gum. *Environ Sci Technol* 43 (23), 8942–8947. <https://doi.org/10.1021/es901897d>.
- Lewis, J., Sjöström, J., 2010. Optimizing the experimental design of unsaturated soil columns. *J Contam Hydrol* 115 (1–4), 1–13.
- Šimůnek, J., Jacques, D., Langergraber, G., Bradford, S.A., Šejna, M., Van Genuchten, M.T., 2013. Numerical modeling of contaminant transport using HYDRUS and its specialized modules. *J Indian Inst Sci* 93 (2), 265–284.

- [41] Bradford, S.A., Yates, S.R., Bettahar, M., Simunek, J., 2002. Physical factors affecting the transport and fate of colloids in saturated porous media, 63-1-63-12 *Water Resour Res* 38 (12). <https://doi.org/10.1029/2002wr001340>.
- [42] Tiraferri, A., Tosco, T., Sethi, R., 2011. Transport and retention of microparticles in packed sand columns at low and intermediate ionic strengths: experiments and mathematical modeling. *Environ Earth Sci* 63 (4), 847–859. <https://doi.org/10.1007/s12665-010-0755-4>.
- [43] Sinha, A., Ischia, G., Menapace, C., Gialanella, S., 2020. Experimental characterization protocols for wear products from disc brake materials (MDPI AG). *Atmosphere* 11 (10). <https://doi.org/10.3390/atmos11101102>.
- [44] Kukutschová, J., Moravec, P., Tomášek, V., Matějka, V., Smolík, J., Schwarz, J., et al., 2011. On airborne nano/micro-sized wear particles released from low-metallic automotive brakes. *Environ Pollut* 159 (4), 998–1006. <https://doi.org/10.1016/j.envpol.2010.11.036>.
- [45] Iijima, A., Sato, K., Yano, K., Kato, M., Kozawa, K., Furuta, N., 2008. Emission factor for antimony in brake abrasion dusts as one of the major atmospheric antimony sources. *Environ Sci Technol* 42 (8), 2937–2942. <https://doi.org/10.1021/es702137g>.
- [46] Amato F. (2018). *Non-Exhaust Emissions: An Urban Air Quality Problem for Public Health. Impact and Mitigation Measure* (Academic Press an imprint of Elsevier (ed.)).
- [47] GÜNEY, B., ÖZ, A., 2020. Taşıt Freni Aşınma Parçacık Emisyonlarının Mikroyapısı ve Kimyasal Analizi. *Eur J Sci Technol* 633–642. <https://doi.org/10.31590/ejosat.744098>.
- [48] Vijay, R., Surya Rajan, B., Sathickbasha, K., Hariharasakthisudhan, P., Lenin Singaravelu, D., Manoharan, S., et al., 2022. Influence of metal sulfide coated steel fibers on the friction and wear performance of brake friction composites. *Tribology Int* 176 (September), 107924. <https://doi.org/10.1016/j.triboint.2022.107924>.
- [49] Peikertová, P., Kukutschová, J., Vávra, I., Matějka, V., Životský, O., Vaculík, M., et al., 2013. Water suspended nanosized particles released from nonairborne brake wear debris. *Wear* 306 (1–2), 89–96. <https://doi.org/10.1016/j.wear.2013.07.008>.
- [50] Bourliva, A., Christophoridis, C., Papadopoulou, L., Giouri, K., Papadopoulos, A., Mitsika, E., et al., 2017. Characterization, heavy metal content and health risk assessment of urban road dusts from the historic center of the city of Thessaloniki, Greece. *Environ Geochem Health* 39 (3), 611–634. <https://doi.org/10.1007/s10653-016-9836-y>.
- [51] McDowell-Boyer, L.M., 1992. Chemical mobilization of micron-sized particles in saturated porous media under steady flow conditions. *Environ Sci Technol* 26 (3), 586–593. <https://doi.org/10.1021/es00027a023>.
- [52] Tosco, T., Tiraferri, A., & Sethi, R. (2009). 2009, 43, 4425–4431. 1, 4425–4431.
- [53] Bueno, V., Bosi, A., Tosco, T., Ghoshal, S., 2022. Mobility of solid and porous hollow SiO₂ nanoparticles in saturated porous media: Impacts of surface and particle structure. *J Colloid Interface Sci* 606, 480–490. <https://doi.org/10.1016/j.jcis.2021.07.142>.
- [54] Legg, B.A., Zhu, M., Comolli, L.R., Gilbert, B., Banfield, J.F., 2014. Impacts of ionic strength on three-dimensional nanoparticle aggregate structure and consequences for environmental transport and deposition. *Environ Sci Technol* 48 (23), 13703–13710. <https://doi.org/10.1021/es502654q>.
- [55] Tosco, T., Bosch, J., Meckenstock, R.U., Sethi, R., 2012. Transport of ferrihydrite nanoparticles in saturated porous media: role of ionic strength and flow rate. *Environ Sci Technol* 46 (7), 4008–4015. <https://doi.org/10.1021/es202643c>.
- [56] Tosco, T., Gastone, F., Sethi, R., 2014. Guar gum solutions for improved delivery of iron particles in porous media (Part 2): iron transport tests and modeling in radial geometry. *J Contam Hydrol* 166 (Part 2), 34–51. <https://doi.org/10.1016/j.jconhyd.2014.06.014>.
- [57] Yao, K.M., Habibian, M.T., O'Melia, C.R., 1971. Water and waste water filtration: concepts and applications. *Environ Sci Technol* 5 (11), 1105–1112. <https://doi.org/10.1021/es60058a005>.
- [58] Shang, J., Flury, M., Deng, Y., 2009. Force measurements between particles and the air-water interface: implications for particle mobilization in unsaturated porous media. *Water Resour Res* 45 (6), 1–14. <https://doi.org/10.1029/2008WR007384>.
- [59] UNECE. (2023). Addendum 24: UN Global Technical Regulation No. 24: Laboratory Measurement of Brake Emissions for Light-Duty Vehicles. 24.
- [60] Varriale, F., Carlevaris, D., Wahlström, J., Malmberg, V., Lyu, Y., 2023. On the impact of pad material ingredients on particulate wear emissions from disc brakes. *Results Eng* 19 (August), 1–7. <https://doi.org/10.1016/j.rineng.2023.101397>.
- [61] Neukirchen, C., Saraji-Bozorgzad, M., Mäder, M., Mudan, A., Czasch, P., Becker, J., et al., 2024. Comprehensive elemental and physical characterization of vehicle brake wear emissions from two different brake pads following the Global Technical Regulation methodology. *J Hazard Mater* 165187. <https://doi.org/10.1016/j.jhazmat.2024.136609>.